

# Developments in the hybrid transformer model – Core modeling and optimization

H. K. Høidalen, N. Chiesa, A. Avendaño, B. A. Mork

**Abstract**—This paper deals with the modeling of power transformers for calculation of switching transients based on mainly test report data. The paper is a follow-up of an IPST'07 paper and discusses the modeling and implementation of core saturation and losses in the Hybrid Transformer. A modified Frolich equation with knee-point adjustment and final slope handling is presented. The optimization process to fit the model to test report data is outlined and the modeling of topologically correct core loss is addressed. The inclusion of type 96 hysteretic inductors is presented. The final slope is a crucial parameter in inrush current calculations and requires design data.

**Keywords:** Power transformers, core modeling, saturation, hysteresis, optimization.

## I. INTRODUCTION

Transformers are critical components in the power system, but their representation in transient studies is often oversimplified. Several modeling approaches are documented in the literature [1] and this paper focuses on models with topologically correct cores. The Hybrid Transformer model [2]-[5] is an engineering transformer model based on limited input data. The modeling of the transformer is based on the magnetic circuit transformed to its electric dual [2], [3]. The leakage and main fluxes are then separated into a core model for the main flux and an inverse inductance matrix for the leakage flux. The copper losses and coil capacitances are added at the terminals of the transformer. The resulting electrical circuit is shown in Fig. 1. Only standard EMTP elements are used.

The model can be based on three sources of data: Design (specify geometry and material parameters of the core and windings), Test report, and Typical (typical values based on the voltage and power ratings). It handles 3-phase transformers with two or three windings. Autotransformers and all Wye and Delta couplings are supported. The model includes an inverse inductance matrix for the leakage description, optional frequency dependent winding resistance, capacitive coupling, and a topologically-correct core model

with individual saturation and losses in legs and yokes. Triplex, 3- and 5-legged and shell-form transformer cores are handled.

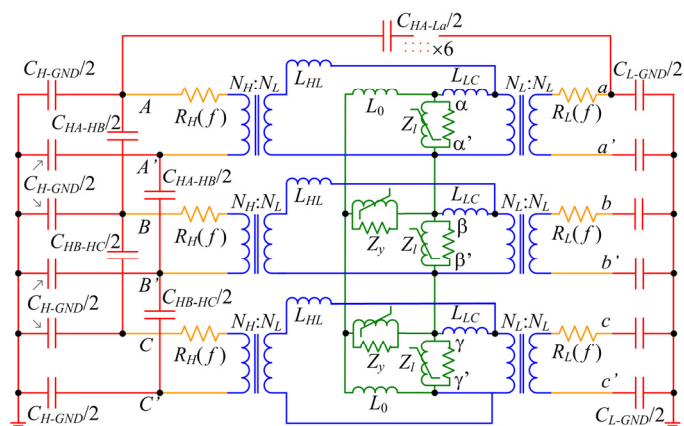


Fig. 1. Electric model of the Hybrid Transformer [4], 2-windings ( $H$  and  $L$ ), 3-phases, 3-legged core.

## II. ENHANCED CORE MODELING

The core saturation curve in the Hybrid Transformer was initially [5] modelled with the Frolich equation as shown in (1).

$$B = \frac{H}{a_m + b_m \cdot |H|} \Rightarrow \lambda'(i) = \frac{i}{a + b \cdot |i|} \quad (1)$$

where the constants  $a = a_m \cdot l_L / (N^2 \cdot A_L)$  and  $b = b_m / (N \cdot A_L)$  are based on the absolute length ( $l_L$ ) and cross section area ( $A_L$ ) of the core leg. The parameter  $a$  controls the slope at low excitations thus  $a_m$  is the inverse of the initial permeability. The parameter  $b$  controls the saturation and  $b_m$  is the inverse of the complete saturation flux density which typically is around 2 T. For other core sections than the leg, the respective core dimensions must be used leading to the general formulation

$$\lambda' / A_r = \frac{i / l_r}{a + b \cdot |i| / l_r} \Leftrightarrow i / l_r = \frac{a \cdot \lambda'}{A_r - b \cdot |\lambda'|} \quad (2)$$

where  $A_r$  and  $l_r$  now are the relative core dimensions referred to the leg. The flux-linkage is as seen in (2), scaled with the area and the current with the length.

The original function (2) is now proposed extended with two new parameters;  $c$  and  $L_\infty$  as shown in (3). The  $c$  parameter improves the fitting to the test report values around the knee area whereas  $L_\infty$  corresponds to the final slope. The two parameters were earlier introduced in [6].

This work was supported by the Norwegian Research Council and SINTEF Energy Research.

H. K. Høidalen is with the Norwegian University of Science and Technology, N-7491 Trondheim, Norway, [hans.hoidalen@elkraft.ntnu.no](mailto:hans.hoidalen@elkraft.ntnu.no).

N. Chiesa is with SINTEF Energy Research, Trondheim, Norway, [Nicola.Chiesa@sintef.no](mailto:Nicola.Chiesa@sintef.no)

B.A. Mork and A. Avendaño are both with Michigan Technological University, Houghton, MI ([bamork@mtu.edu](mailto:bamork@mtu.edu), [aavedano@mtu.edu](mailto:aavedano@mtu.edu))

Paper submitted to the International Conference on Power Systems Transients (IPST2011) in Delft, the Netherlands June 14-17, 2011

$$\lambda(i) / A_r = \frac{i / l_r}{a + b \cdot |i| / l_r + c \cdot \sqrt{|i| / l_r}} + L_\infty \cdot i / l_r \quad (3)$$

The final slope is in the magnetic case equal to  $\mu_0$  and in the electrical case this transfers to

$$L_\infty = \mu_0 \cdot N^2 \cdot \frac{A_L}{l_L} = \mu_0 \cdot a_m / a \quad (4)$$

While  $a$ ,  $b$ , and  $c$  can be obtained from test-report data in a fitting process, as described next, the  $L_\infty$  parameter has to be based on design parameters.  $L_\infty$  is a very crucial parameter for inrush calculations as seen in [7]. Air-core inductance can be provided by manufacturer and is used in analytical inrush current calculations. In the Hybrid Transformer this air-core inductance is split between the standard leakage inductance, the additional leakage between the inner winding and the core and the final slope inductance. The actual splitting is dependent on the width of the windings [7].

One drawback with the new formulation in (3) is that an analytical inverse function for the current, given the flux-linkage cannot be easily obtained (in contrast to (2)). A numerical approach using Newton's method is used in the Hybrid Transformer, using the analytical current at  $c=0$  as a starting point.

$$i(\lambda) = g(\lambda, a, b, c | l_r, A_r, L_\infty) \quad (5)$$

### III. OPTIMIZATION METHODS

The Hybrid Model uses an optimization strategy in order to obtain the  $a$ ,  $b$ , and  $c$  values in (3) from the open circuit test report. An object function is defined as shown in (6) where the  $a$ ,  $b$ , and  $c$  values minimizing this function is searched for.

$$F(a, b, c) = \sum_{\substack{V= \\ \text{excitation} \\ \text{levels}}} \left( 1 - \frac{I_{rms,calc}(a,b,c,V)}{I_{rms,meas}(V)} \right)^2 \quad (6)$$

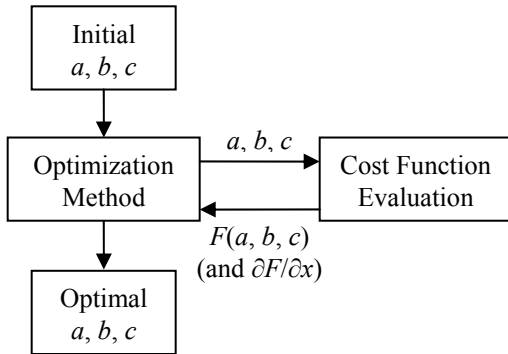


Fig. 2. Optimization principle.

In [5] a Golden Search method [8] was used. This approach involved sequential and iterative search for optimal ( $a$ ,  $b$  (and  $c$ )) values. The main challenge with this approach was the discontinuous current function in (2), where for  $\lambda' \geq A_r / b$  there exists no current solution. This was further

complicated when the parameter  $c$  was introduced. To increase the robustness of the optimization routine a Genetic Algorithm [9] was later introduced. Such a routine is good at handling discontinuities but is on the other hand rather slow. Furthermore it was observed that the routine had a tendency to arrive at not exactly reproducible results even if the random generator was carefully reset.

The introduction of the  $L_\infty$  parameter in (3) has the big advantage that the inverse function in (5) (although not analytical) becomes continuous with an always existing derivative. This enables the introduction of a gradient based method. The L-BFGS-B routine [10] (limited memory algorithm for bound constrained optimization) which is a quasi-Newton method with numerical calculation of the gradient was chosen. The routine requires evaluation of the cost function and its derivatives with respect to the variables ( $a$ ,  $b$ ,  $c$ ). The gradient is calculated based on the central difference formula:

$$\frac{\partial F}{\partial x} \approx \frac{F(x+h) - F(x-h)}{2h} \quad (7)$$

where  $x$  is the variable ( $a$ ,  $b$  or  $c$ ) and the discretization interval  $h = 10^{-6}$ . If  $n$  is the number of variables in the optimization problem the cost function thus has to be evaluated  $2n+1$  times for each solution point. The iteration number is somewhat loosely defined in the routine. If the solution is poorer than the previous point the algorithm steps backwards along the gradient until an improved solution is found and only then the iteration number is incremented. The routine arrives always to the same (local) minimum point with the same starting point so reproducibility is achieved. There is a guarantee for a real global minimum only if the problem is convex without local minima. All tests show that this is the case for the problem in (6) although this has not been mathematically proven. The time consumption for arriving at a minimum went down from around 30 seconds (with the Genetic Algorithm) to 1 second (with the Gradient Method).

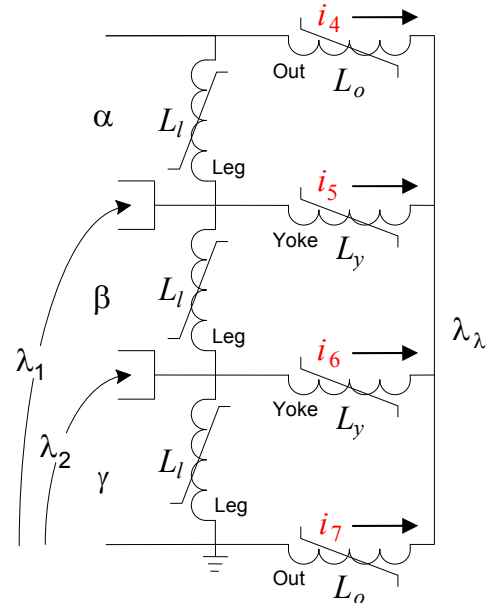


Fig. 3. 5-legged core model [2]

For a single phase core (triplex) and also a shell form core the cost function is easily formulated [2] and its calculation is fast. But for a 3-legged core with zero-sequence paths considered and a 5-legged core (Fig. 3) the optimization process is complicated. Calculation of the rms value of the currents flowing into the core windings  $\alpha\beta\gamma$  with known flux-linkage sources  $\lambda_1$  and  $\lambda_2$  (and guessed  $a, b, c$  values) requires calculation of the neutral flux  $\lambda_\lambda$ . This flux is found from the boundary equation [2]:

$$i_4 + i_5 + i_6 + i_7 = 0 \quad (8)$$

which based on (5) and Fig. 3 is composed of

$$\begin{aligned} i_4 &= g(-\lambda_\lambda, a, b, c | l_{ro}, A_{ro}, L_\infty) = i_7 \\ i_5 &= g(\lambda_1 - \lambda_\lambda, a, b, c | l_{ry}, A_{ry}, L_\infty) \\ i_6 &= g(\lambda_2 - \lambda_\lambda, a, b, c | l_{ry}, A_{ry}, L_\infty) \end{aligned} \quad (9)$$

with

$$\begin{aligned} \lambda_1 &= -\sqrt{2} \cdot V_i / \omega \cdot \sin(\omega t) \\ \lambda_2 &= \sqrt{2} \cdot V_i / \omega \cdot \sin(\omega t + 2\pi/3) \end{aligned} \quad (10)$$

From the boundary equation (8) the neutral flux-linkage  $\lambda_\lambda$  is found iteratively using Newton's method. For a 5-legged core this flux-linkage looks typically (with rated values from Table I) as shown in Fig. 4, while for a 3-legged core it is very close to zero. The neutral flux-linkage is symmetrical around  $2\pi/3$  and this is utilized in the calculation to increase the calculation speed.

The calculation of the neutral flux-linkage  $\lambda_\lambda$  is the most time consuming part of the optimization process. As shown in Fig. 5 the calculation has to be performed in the inner loop of the cost function evaluation and is thus time-critical.

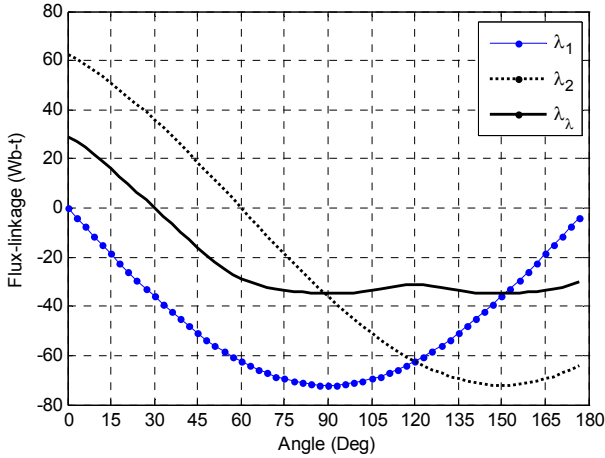


Fig. 4. Flux-linkages in a 5-legged core. The flux-linkages  $\lambda_1$  and  $\lambda_2$  are the two sources used in the calculation, while  $\lambda_\lambda$  is the neutral flux-linkage.

#### IV. CORE LOSS MODELING

Core loss modeling is a topic that still requires more research. Separation of losses in eddy-current, hysteresis and excess losses and the further separation into sections of the core is complicated [11, 12]. The original implementation [5] had several weaknesses in its core loss representation.

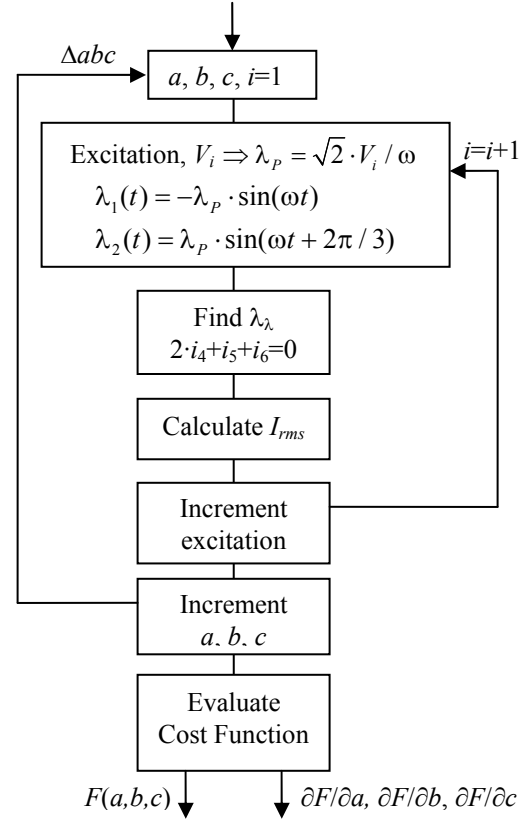


Fig. 5. Cost function evaluation process.

#### A. Hysteresis

Evaluation of inrush currents requires the magnetization inductances to be initialized according to the residual flux. The implemented Hybrid Model [5] did not allow initialization, however. The approach with resistors representing the core loss in parallel to the magnetization inductance will also prevent the model arriving at residual flux. In [7] a true hysteretic core model based on Jiles-Atherton theory was used. Such a model is however very demanding when it comes to computational resources, numerical issues, and parameter estimation. Even the complicated Jiles-Atherton model (with constant parameters at least) did not represent core losses well with increasing excitation. Here, a more simplistic approach is suggested where a type 96 hysteretic inductor is used instead.

The core loss is split in two equal parts. One part is attributed to eddy current losses and are included in a parallel resistor. The other half is assigned to hysteresis losses and is included in the type 96 component. The hysteresis losses  $P_H$  are further scaled to the maximum excitation with a Steinmetz coefficient of 2 as shown in (11) which seems reasonable according to [11].

$$P_H = \frac{P}{2} \cdot \left( \frac{\lambda_{\max}}{\lambda_{\text{rated}}} \right)^2 \quad (11)$$

where  $P$  is the rated core loss (at  $\lambda_{\text{rated}}$ ) for the involved section of the core.  $\lambda_{\max}$  is the final point of the hysteresis loop as shown in Fig. 6.

The width of the hysteresis loop is assumed to be constant

(but goes to zero at the second highest flux-linkage point) and calculated as

$$W = \frac{P_H}{f \cdot (\lambda_{np-1} + \lambda_{np-2})} [A] \quad (12)$$

where  $f$  is the power frequency and the flux-linkages  $\lambda_{np-1}$  and  $\lambda_{np-2}$  are given in the piece-wise nonlinear curve of Fig. 6 and their sum multiplied by the width  $W$  becomes the area of the hysteresis loop.

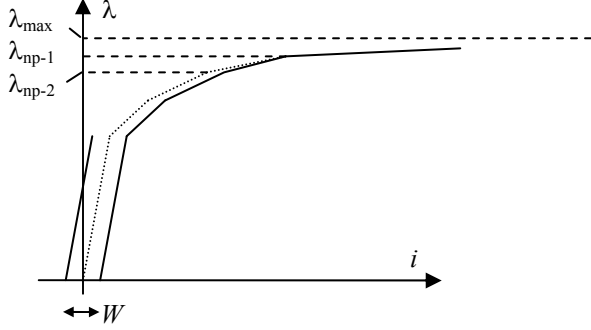


Fig. 6. Construction of the hysteresis curve in the type 96 component.

### B. Core loss topology

The inductive and resistive parts of the core were in the original Hybrid Model separated both in the evaluation and modeling as shown in Fig. 7a). This type of modeling approach manages to reproduce rated test report values, although the linear resistor approach only is reasonable for a rather narrow band of excitations. The topology is however not correct and this can have some significant consequences for unbalanced excitations. In general, the aim should therefore be to establish a core model as shown in Fig. 7b). This is also required to use the hysteresis approach described above.

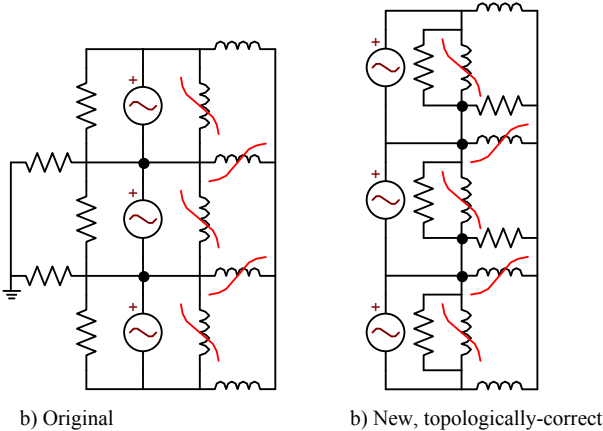


Fig. 7. 3-legged core model with a) artificial inductive and resistive separation (left), and b) Topological correct core losses (right).

The core loss is split in parts associated with individual core sections. A basic assumption in [5] was that the core loss in a section is proportional to the volume of that section. And further that the equivalent core loss resistance was inversely proportional to the section loss, assuming a constant voltage

across each element. This last assumption does not hold, however, at least not for a 5-legged core where the voltage across the yoke branch is different from the leg branch.

In this paper it is proposed to let the core loss also change with the flux density and a Steinmetz coefficient of two is proposed. The flux density is further assumed proportional to the rms value of the voltage across the section. This gives the loss in a section

$$P_r \sim A_r \cdot l_r \cdot V_r^2 \quad (13)$$

where  $A_r$  and  $l_r$  are the relative area and core section length,  $V_r$  is the ratio of the rms voltage across the section and across the leg (excitation voltage). Now, let the loss in the leg section be  $P_{leg}$  and the total measured core loss  $P_{meas}$ . This gives losses in section:

$$P_r = P_{leg} \cdot A_r \cdot l_r \cdot V_r^2 \quad (14)$$

$$P_{leg} = \frac{P_{meas}}{3 + 2 \cdot A_{ry} \cdot l_{ry} \cdot V_{ry}^2} \quad (15)$$

for a 3-legged core (3 legs and 2 yokes) and

$$P_{leg} = \frac{P_{meas}}{3 + 2 \cdot A_{ry} \cdot l_{ry} \cdot V_{ry}^2 + 2 \cdot A_{ro} \cdot l_{ro} \cdot V_{ro}^2} \quad (16)$$

for a 5-legged core (3 legs, 2 yokes, 2 outer legs)

The resistance representing core losses in each section can now generally be written as

$$R_r = \frac{V_i^2}{P_{leg} \cdot A_r \cdot l_r} \quad (17)$$

where  $V_i$  is the voltage across the leg (excitation). Only the rated excitation is utilized in this paper and the resistance is assumed to be constant. This is the same formulation as in [5] and the only difference lies in the calculation of the leg losses in (15) and (16).

The challenge here is of course to determine the voltage across the yoke and outer leg sections. This involves working with the time derivatives of the fluxes in Fig. 4.

## V. RESULTS

The same test object as used in [5] is also used here as given in Table I. This is a 5-legged, 290 MVA GSN transformer where extended test report measurements are available, but no design information.

TABLE I  
GENERATOR STEP-UP TRANSFORMER TEST REPORT

Main data	[kV]	[MVA]	[A]	Coupling
HS	432	290	388	YNj
LS	16	290	10465	d5
Open-circuit	$E_0$ [kV, (%)]	[MVA]	$I_0$ [%]	$P_0$ [kW]
LS	12 (75)	290	0.05	83.1
	14 (87.5)	290	0.11	118.8
	15 (93.75)	290	0.17	143.6
	16 (100)	290	0.31	178.6
	17 (106.25)	290	0.67	226.5
Short-circuit	[kV]	[MVA]	$ek, er$ [%]	$P_k$ [kW]
HS/LS	432/16	290	14.6, 0.24	704.4

Fig. 8 shows the open circuit response of the proposed model as compared to the test report given in Table 1 and the XFMR and UMEC models investigated in [5]. The model in this paper gives somewhat reduced magnetization current for over-excitation than the similar model in [5]. This is because the final slope attribute has been added in this paper. The response still gives much higher current than the UMEC approach which in [5] used linear extrapolation beyond the last test report point.

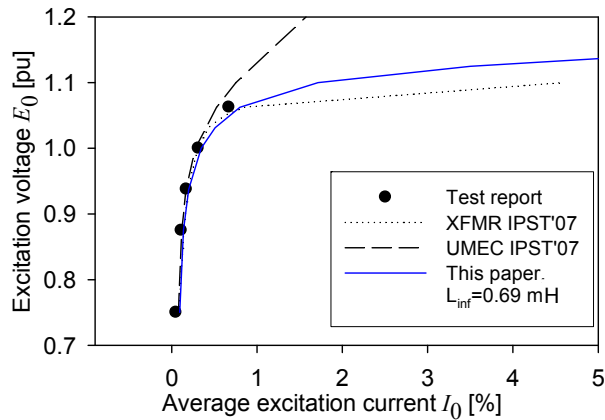


Fig. 8 Model performance open circuit excitation, compared to test report and the investigation in [5].

Fig. 9 shows the inrush current for the proposed model compared to [5]. Simple piece-wise linear inductors (type 98) are used in this case and rated voltage is connected at the voltage zero crossing of phase A (worst case). As observed in the figure the inrush current is even higher in this model compared to the XFMR model in [5] even if the saturation in Fig. 8 apparently is higher. However, the final slope is actually lower in the proposed model and crosses the XFMR curve from [5] at very high excitations. The reason is that too little attention was paid to the final slope in [5] and that an artificial final slope was created in the conversion from the Frolich equation to a piece-wise linear curve. This also illustrates how critical the final slope is for the simulation of inrush currents.

Fig. 10 shows the calculated core losses compared to the test report values in Table I. The core loss matches perfectly at 1 pu excitation because this value is used in the fitting. The model does not show a so pronounced variation of the losses with excitation as the measurements. This is because a constant core loss resistance is used based on rated values.

Using hysteretic inductors in the simulation can result in biased residual fluxes and a significant increase in the inrush currents. The type 98 inductors used for the simulation in Fig. 9 were changed to hysteretic inductors type 96 embedding half of the core losses. The switching instant was the same except for a one period (20 ms) ramp-up time required to tune in the type 96 inductors; The switch opens at the zero crossing of phase voltage A and closes 40 ms later. As seen in Fig. 11 the inrush current is reduced in this case since the residual flux is negative and opposing the current.

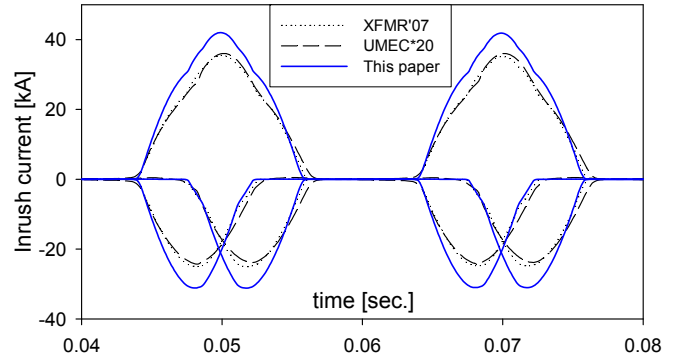


Fig. 9 Calculation of inrush currents compared to [5]. Switching in with zero residual flux at the zero crossing of phase A voltage.

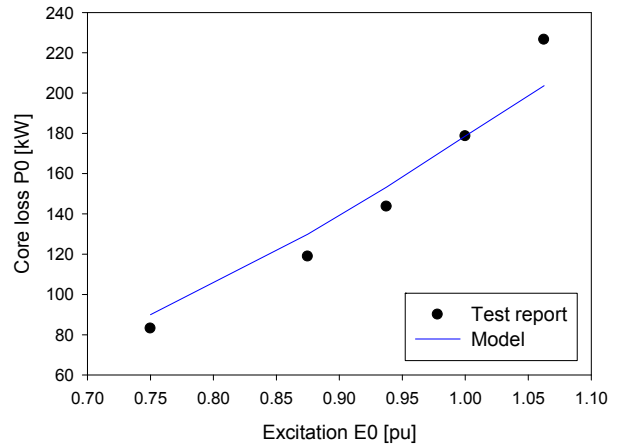


Fig. 10. Core loss as a function of excitation level.

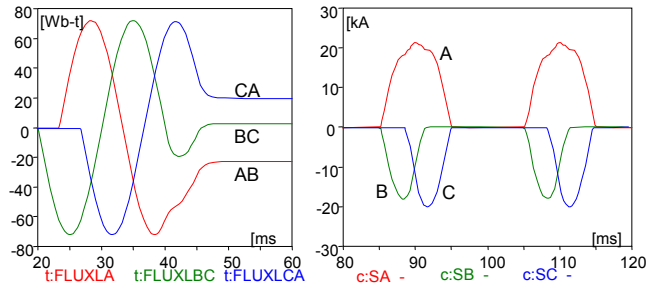


Fig. 11. Effect of using hysteretic inductors (type 96). Integral of line-voltage LV side (left) and inrush currents (right).

The approach in (14) for calculating the losses in each core section requires the voltage across the sections. These are found by taking the derivative of the flux-linkage differences. In this process it is assumed that the core loss resistors do not contribute to the core voltage balance. Fig. 12 shows the calculated core voltages of the complete model and the yoke flux-linkage found by integrating the yoke voltage.

## VI. DISCUSSION

The inclusion of the final slope of the saturation curve is critical for the accuracy of inrush calculations. The value of this parameter should be based on design information and is entered separately. Estimation based on (4) requires the  $a_m$

magnetic material data parameter and the  $a$  parameter which is prone to fitting errors. Moreover, the final slope when added to the Frolic equation (3) enables a much faster fitting process by enabling the usage of a gradient method even if the involved functions (9) are not easily analytically obtainable.

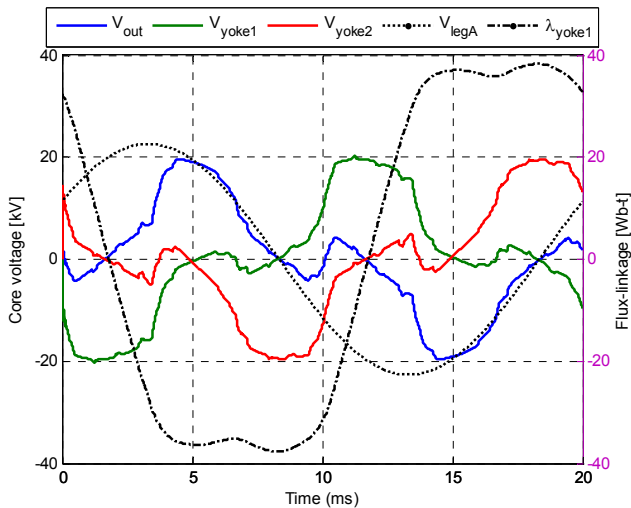


Fig. 12. Core voltages across the yoke ( $V_{YOKE1}$  and  $V_{YOKE2}$ ), outer leg ( $V_{OUT}$ ), and the leg ( $V_{LEGA}$ ), along with the flux-linkage in yoke 1 ( $\lambda_{yoke1}$ ).

The inclusion of a hysteretic type 96 inductor in the core is considered to be just an intermediate step in the model development. Such model is capable to arrive at residual flux after de-energization, as seen in Fig. 11, but is not good for transient analysis. The 50 % split between hysteresis and eddy current losses (ignoring anomalous losses) can be discussed likewise the assumed rms voltage section loss dependency. There is a tendency that hysteresis losses are smaller for modern core materials. Likewise the hysteresis losses depend on the average rather than the rms value of the voltage [12].

The voltage in the core model is assumed to be governed by the flux alone and the actual interaction between the inductive and resistive elements is ignored. Fig. 12 shows simulated core voltage waveforms but these are not available in the parameter estimation process. As seen when comparing Figs. 4 and 12, the actual flux-linkage is somewhat larger than the estimated indicating that the core resistors will influence the core voltage distribution and thus the flux. A harmonic analysis of the core voltages in Fig. 12 showed that these voltages contain a large amount of 3<sup>rd</sup> harmonics (~53 %). This will complicate the core loss modeling even further as the split between eddy current and hysteresis losses is frequency dependent [12].

## VII. CONCLUSION

The Hybrid Transformer Model is enhanced with an improved core model. This involves

- Final slope of the saturation curve. Design parameters (absolute core leg dimensions and turn number) are required to estimate the value.
- Topologically-correct core loss representation by consideration of flux density and core section voltage.
- A hysteretic core model which enables residual flux and

self-initialization.

The inclusion of the final slope also enabled a much faster optimization process for test report fitting. All features described in this paper are implemented in ATPDraw ver. 5.6.

## VIII. REFERENCES

- [1] J. A. Martinez and B. A. Mork, "Transformer modeling for low- and mid-frequency transients – a review", *IEEE TPWRD*, vol. 20, no. 2, pp. 1625-1632, April 2005.
- [2] B. A. Mork, F. Gonzalez, and D. Ishchenko: "Parameter estimation and advancements in transformer models for EMTP simulations. Task MTU-7: Model performance and sensitivity analysis", Bonneville Power Administration, Portland, OR, 2004.
- [3] B.A. Mork, F. Gonzalez, D. Ishchenko, D. L. Stuehm, J. Mitra." Hybrid Transformer Model for Transient Simulation-Part I: Development and Parameters", *IEEE TPWRD*, Vol. 22, pp. 248-255, Jan. 2007.
- [4] B.A. Mork, F. Gonzalez, D. Ishchenko, D. L. Stuehm, J. Mitra, "Hybrid Transformer Model for Transient Simulation-Part II: Laboratory Measurements and Benchmarking", *IEEE TPWRD*, Vol. 22, pp. 256-262, Jan. 2007
- [5] H. K. Hoidalen, B. A. Mork, F. Gonzalez, D. Ishchenko, N. Chiesa: "Implementation and verification of the Hybrid Transformer model in ATPDraw", *Proc. IPST'07*, Lyon, France, June 3-7, 2007.
- [6] N. Chiesa, H. K. Hoidalen, "Hysteretic iron-core inductor for inrush current modeling in EMTP", 16<sup>th</sup> PSCC, Glasgow-UK, Jul. 2008.
- [7] N. Chiesa, B.A. Mork, H. K. Hoidalen, "Transformer model for inrush calculations: Simulation, measurements and sensitivity analysis", *IEEE TPWRD*, Vol. 5, pp. 2599-2608, Oct. 2010.
- [8] W. H. Press, S. A. Teukolsky, W. T. Vetterling, B. P. Flannery: Numerical recipes, 2nd Ed. 1992, Cambridge University Press.
- [9] www.RiverSoftAVG.com, The Genetic Algorithm (GA).
- [10] C. Zhu, R.H. Byrd and J. Nocedal: L-BFGS-B: Algorithm 778: L-BFGS-B, FORTRAN routines for large scale bound constrained optimization, *ACM Transactions on Mathematical Software*, Vol 23, Num. 4, 1997 Page(s): 550 – 560.
- [11] F. De Leon, A. Semlyen: "A simple representation of dynamic hysteresis losses in power transformers", *IEEE TPWRD*, Vol. 10, pp. 315-321, Jan. 1995.
- [12] N. Chiesa, Power Transformer Modeling for Inrush Current Calculation, PhD dissertation NTNU, April 2010, ISBN- 978-82-471-2086-6

## IX. BIOGRAPHIES

**Hans Kr. Hoidalen** was born in Norway in 1967. He received his MSc and PhD from the Norwegian University of Science and Technology in 1990 and 1998 respectively. He is now a professor at the same institution with a special interest of electrical stress calculations and modeling.

**Nicola Chiesa** was born in Italy in 1980. He received the M.Sc. degree in electrical Engineering from Politecnico di Milano in 2005, and the PhD degree from the Norwegian University of Science and Technology in 2010. He is now a research scientist at SINTEF Energy Research.

**Aleandro Avendano** was born in Tijuana, México in 1982. He received the B.S. degree in Electromechanical Engineering from Instituto Tecnológico de Tjuana in 2004. In 2005 he was awarded with a scholarship from the National Science and Technology Council of Mexico (CONACYT) and joined the Department of Electric & Computer Engineering at Michigan Technological University. He is now a Ph.D. candidate at MTU.

**Bruce A. Mork** was born in ND-USA in 1957. He received the BSME, MSEE, and PhD from North Dakota State University in 1979, 1981 and 1992 respectively. He joined the faculty of Michigan Technological University in 1992, where he is now Professor of Electrical Engineering, and Director of the Power & Energy Research Center.